

PACS numbers: 79.20.Ds; 36.40.–c; 52.38.Mf; 81.07.–b
DOI: 10.1070/QE2010v040n11ABEH014443

Pulsed laser ablation of binary semiconductors: mechanisms of vaporisation and cluster formation

A.V. Bulgakov, A.B. Evtushenko, Yu.G. Shukhov, I. Ozerov, W. Marine

Abstract. **Formation of small clusters during pulsed ablation of two binary semiconductors, zinc oxide and indium phosphide, in vacuum by UV, visible, and IR laser radiation is comparatively studied. The irradiation conditions favourable for generation of neutral and charged Zn_nO_m and In_nP_m clusters of different stoichiometry in the ablation products are found. The size and composition of the clusters, their expansion dynamics and reactivity are analysed by time-of-flight mass spectrometry. A particular attention is paid to the mechanisms of ZnO and InP ablation as a function of laser fluence, with the use of different ablation models. It is established that ZnO evapourates congruently in a wide range of irradiation conditions, while InP ablation leads to enrichment of the target surface with indium. It is shown that this radically different character of semiconductor ablation determines the composition of the nanostructures formed: zinc oxide clusters are mainly stoichiometric, whereas In_nP_m particles are significantly enriched with indium.**

Keywords: *laser ablation, clusters, binary semiconductors, zinc oxide, indium phosphide, congruent vaporisation, nonthermal particle emission, mass spectrometry.*

1. Introduction

Nanoclusters and nanomaterials based on binary semiconductors (ZnO, InP, CdTe, SiO, etc.) attract increasing attention in view of their current and potential applications in very diverse fields of research and technology [1 – 4]. A far from complete list of these fields includes catalysis, nanoelectronics, optoelectronics devices and sensors, solar power engineering, and medicine. Due to the well-developed surface (almost all atoms in a 1-nm particle are surface ones) and the quantum confinement effect [5], nanoscale semiconductors have unique optical, electronic, catalytic, and other properties, which are attractive for various applications. For example, solar cells based on nanoscale cadmium telluride demonstrate a record solar energy conversion efficiency [6] and are considered as more promising for commercial application than conventional silicon solar cells [7]. Indium phosphide nanocrystals have a high photoluminescence efficiency in a wide spectral range [8]. Nanostructured zinc oxide is one of the most promising materials for field emitters [9], UV optoelectronic devices [3, 10], and nanolasers [11, 12].

Nanoclusters and nanomaterials are produced by different methods: gas-dynamic, chemical, plasma, and beam [13 – 15]. One of the most promising techniques of cluster synthesis is pulsed laser ablation (PLA). Its main advantage is the possibility of excluding the presence of foreign impurities in the nanostructures synthesised, which is especially important for applications (one foreign atom in a 2-nm particle corresponds to a defect concentration of $\sim 10^{21}$ cm^{-3} and can radically change the particle properties). The other advantages of PLA are its flexibility and possibility of monitoring the cluster growth. Nanoclusters can be formed during PLA according to two different scenarios: (i) aggregation of the initial ablation products (atoms, molecules) in the expanding laser plasma and (ii) direct emission of clusters from the irradiated surface. Recently significant progress has been made in the PLA synthesis of nanoclusters of one-component semiconductors with controlled size, shape, and optical properties [16, 17], as well as in understanding and quantitative description of cluster formation [18 – 20]. The situation with multicomponent nanostructures is less clear. Although recently PLA has been widely applied to synthesise nanoclusters of binary semiconductors [8, 21 – 23], their formation during PLA has been insufficiently studied; correspondingly, it is a serious problem to obtain nanoclusters with specified properties. An additional difficulty is that, along with the size of clusters, their composition (which radically affects their optical, electronic, and structural properties [15]) has also to be controlled. Moreover, varying the composition, one can stabilise multicomponent nanoclusters of a certain size [24].

The size and stoichiometry of multicomponent PLA-produced nanoclusters depend strongly on the ablation conditions, in particular, on the laser intensity and wavelength and on the ambient gas parameters (type, pressure, and temperature) [21, 25 – 28]. A serious problem in the application and analysis of PLA of multicomponent materials is the possibility of target deviation from stoichiometry during irradiation because of the different volatility of target components (the so-called incongruent vaporisation). In this case, the target surface is enriched with the less volatile component during irradiation, resulting in a change in the thermophysical and optical properties of the target material. The effect of incongruent vaporisation of multicomponent materials upon their thermal heating (thermal decomposition) has been known for more than 100 years; the fundamental studies in this field were carried out by Hertz, Knudsen, Langmuir, and Arrhenius [29]. With respect to the character of thermal vaporisation, binary semiconductors are divided into two types. Some of

A.V. Bulgakov, A.B. Evtushenko, Yu.G. Shukhov S.S. Kutateladze Institute of Thermophysics, Siberian Branch, Russian Academy of Sciences, prosp. akad. Lavrent'eva 1, Novosibirsk, 630090, Russia; e-mail: bulgakov@itp.nsc.ru;
I.Ozerov, W.Marine Université de la Mediterranée, CINaM, UPR CNRS 3118, Marseille, France

Received 19 August 2010
Kvantovaya Elektronika **40** (11) 1021 – 1033 (2010)
Translated by Yu.P. Sin'kov

them (e.g., ZnO) evapourate congruently in a wide temperature range [30], whereas the others (for example, InP [31], CdTe [32], or GaAs [33]) lose mainly a more volatile component upon heating above some limiting temperature.

The mechanism of incongruent vaporisation is still discussed even for such a relatively simple process as thermal heating [34]. In the case of PLA, the analysis of vaporisation is hindered because it is an essentially nonstationary process, where, along with the thermal mechanism, nonthermal desorption, electronic excitation of the sample, defect formation under multiple irradiation, and other effects may manifest themselves [35]. Incongruent vaporisation was observed for PLA of some binary semiconductors [36–39] and alloys [40]. Obviously, the change in the composition of the irradiated surface plays a fundamental role in the PLA-induced nanocluster formation and laser deposition of multicomponent films. The data in the literature on the composition of binary semiconductor clusters in PLA products are rather contradictory. For example, off-stoichiometric (zinc-rich) Zn_nO_m clusters were detected during ablation of zinc oxide in [41], whereas in other studies stoichiometric [42] and even oxygen-rich [43] clusters were observed under similar conditions.

In this paper, we report the results of studying the formation of small clusters during PLA of two binary semiconductors (zinc oxide and indium phosphide) in vacuum. The ablation was performed by nanosecond IR (1064 nm), visible (532 nm), and UV (193 nm) laser pulses and by 800-nm femtosecond laser pulses. Data on the size, composition, and reactivity of neutral and charged clusters for different irradiation conditions were obtained by time-of-flight (TOF) mass spectrometry. A particular attention has been paid to the mechanisms of InP and ZnO ablation as a function of laser fluence. The data on the InP ablation depth were analysed within both thermal and nonthermal ablation models. It is shown that under IR and visible light pulses zinc oxide is vaporised congruently, which facilitates the formation of stoichiometric $(ZnO)_n$ clusters in the laser plume. On the contrary, during ablation of indium phosphide the target surface is enriched with indium, and the composition of the produced clusters significantly deviates from stoichiometry. The expansion dynamics of different plume components and the change in the composition of the ablation products during target irradiation are analysed. An effect of delayed phosphorus vaporisation during InP ablation is revealed. The influence of the mechanism of laser vaporisation, character of ablation product expansion, and the laser wavelength on the cluster formation is discussed.

2. Experimental

The ablation experiments were performed with two samples of binary semiconductors: a polycrystalline sintered ZnO target and an InP(100) single crystal; the residual gas pressure during the experiments was 10^{-5} Pa. Four different laser systems, operating at the wavelengths λ = 1064 nm (Nd:YAG laser, pulse width 9 ns), 532 nm (second harmonic of Nd:YAG laser, 7 ns), 193 nm (ArF laser, 15 ns), and 800 nm (Ti:sapphire laser, 100 fs), were used for ablation. In all cases laser pulses had a Gaussian temporal profile, and the aforementioned pulse widths corresponded to the pulse FWHM. The laser radiation was focused by a lens on the target surface in a spot with an area of ~0.5 mm^2 (determined at a level of $1/e^2$). The laser fluence on the target, F_0, was varied in the ranges of 0.3–8 and 0.05–1 J cm^{-2} for ZnO and InP, respectively. The target was placed in a vacuum chamber on a rotating holder (to exclude the formation of a surface crater under multipulse irradiation).

The study was based on a mass spectrometric analysis of the relative concentrations and velocities of different particles in the ablation plume. A general scheme of the experiment is shown in Fig. 1. The ablation products expanded into vacuum in the field-free space toward the ion source of the TOF mass spectrometer. The design of the system makes it possible to independently analyse the charged and neutral particles in the plume. In the latter case the plasma intrinsic ions were cut off from the ion source using deflection plates (DP-1 in Fig. 1; electric field strength 150 V mm^{-1}). Neutral particles were ionised at a distance of 6 cm from the target by an electron impact (electron energy 90 eV, pulse width 1 μs) or an ArF laser pulse (193 nm, 5 ns). The ions formed (or intrinsic charged plasma particles) were repelled by a high-voltage pulse in the transverse direction, passed through a system of deflection plates (DP-2), and entered the drift field of the mass spectrometer. The plume expansion dynamics was analysed based on the TOF distributions of particles, obtained by varying the delay time τ between the ionisation pulse and ablation laser pulse.

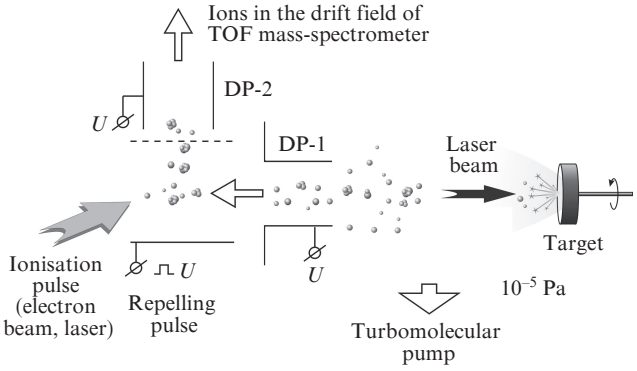

Figure 1. Schematic of the experiment (DP-1 and DP-2 are deflection plates).

The mass spectrometer used (of a mass-reflectron type) had a dynamic range up to 8000 amu and a resolution of ~1000, which made it possible to distinguish between Zn_nO_m and $Zn_{n\pm1}O_{m\mp4}$ clusters by the isotopic distribution of zinc atoms and identify hydrogenated clusters. The clusters were analysed using a special ion filter (mounted in front of the mass-spectrometer detector) to cut off the dominant atomic ions (Zn^+ or In^+) and thus avoid detector saturation. The detector was an assembly of three microchannel plates in a chevron configuration. The detector signal was amplified by a Novelec AD100B broadband amplifier and collected with a Tektronix TDS 5034 digital oscilloscope. All the mass-spectrometric data (unless otherwise specified) were obtained by averaging over 150–200 laser pulses. The experimental setup details were described in [20, 27, 44–46].

We performed mass-spectrometric studies of three types: (i) analysis of the relative particle concentrations in the laser plume as a function of the irradiation conditions, (ii) study of the expansion dynamics of the main plume particles, and (iii) measurements of the individual particle yields as functions of the number of laser pulses irradiating the same point on the

target surface. In addition, in the case of ablation of InP, the total removed mass was measured by weighing the target before and after irradiation with many (10^4–10^5) laser pulses, using a GH-202-A&D precision balance (measurement error 10 μg). The weighting measurements were used to calibrate the mass-spectrometric data (integral of TOF distributions) in order to determine the particle yield at low laser fluences.

3. Analysis of ablation mechanisms

In this section we consider the mechanisms of ablation of binary semiconductors by an example of InP ablation using nanosecond laser pulses (λ = 532 nm), based on the experimental data on the mass removal (ablation depth). The experiments were performed under multipulse irradiation, when the concentration ratio of indium to phosphorus in the ablation products reaches a constant value, corresponding to congruent vaporisation (see Subsection 4.3). Therefore, to estimate the ablation depth from the mass-spectrometric data, we performed measurements only for indium atoms, whose detection sensitivity greatly exceeds that of phosphorus particles. Figure 2 shows the average ablation depth, Z_0, found by weighting and from mass-spectrometry data (in the latter case both electron-impact and laser ionisation techniques were used). For clarity, the data are given in lattice monolayers (MLs) (1 ML ≈ 1.8 ng mm^{-2}) removed per pulse. A conventional boundary of the transition to the developed ablation corresponds to removal of 1 ML [35]; under the given conditions this occurs at $F_0 \approx 170$ mJ cm^{-2}. At higher laser fluences the number of particle collisions in the plume becomes fairly large, and one might expect cluster formation as a result of particle aggregation.

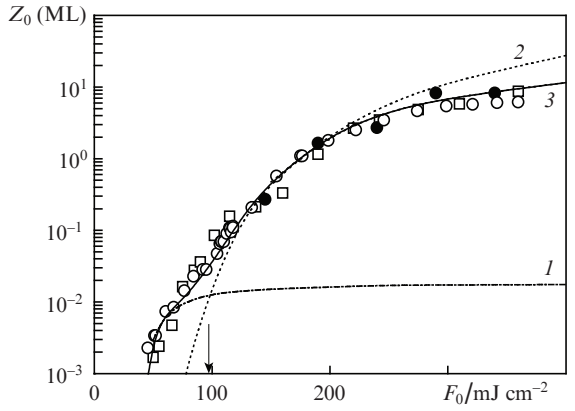

Figure 2. The average InP ablation depth as a function of the fluence of 532-nm laser radiation. Symbols indicate the experimental data obtained by mass-spectrometry with (□) electron-impact and (○) laser ionisation and (●) by weighting. The curves show the results of the calculations within (*1*) the model of nonthermal emission [68] and (*2*) the thermal model with plasma screening disregarded and (*3*) the total ablation depth calculated in terms of the thermal and nonthermal models taking into account screening (see details in the text).

It is natural to analyse the obtained dependence $Z_0(F_0)$ within the thermal model, which is the most developed ablation model [35, 47–51]. It implies that the laser action on a target is reduced to its thermal heating, which is described by the time-dependent heat-conduction equation. In the one-dimensional approximation (valid for many situations [50]) and in the coordinate system related to the moving vaporisation front, this equation has the form

$$c\rho\left[\frac{\partial T}{\partial t} - u(t)\frac{\partial T}{\partial z}\right] = \frac{\partial}{\partial z}\lambda_T \frac{\partial T}{\partial z}$$

$$+(1-R)\alpha_b I(t)\exp(-\alpha_b z) \qquad (1)$$

with the boundary conditions

$$T(z,0) = T_0,\ T(0,t) = T_s,\ \lambda_T \frac{\partial T}{\partial z}\bigg|_{z=0} = Lu(t), \qquad (2)$$

where c is the specific heat; ρ is the density; λ_T is the thermal conductivity; R is the reflectance; α_b is the absorption coefficient; $I(t)$ is the radiation intensity on the surface; L is the latent heat of vaporisation; and $u(t)$ is the vaporisation front velocity (ablation rate), which is determined by the sum of the mass fluxes j_i of individual components from the surface [52, 53]:

$$u(t) = \frac{1}{\rho}\sum_i j_i. \qquad (3)$$

The thermal model generally implies surface (normal) vaporisation; thus, the flux of material removed from the surface can be found from the Hertz–Knudsen equation [50–55]:

$$j_i(T_s) = (1-\beta)p_i(T_s)\sqrt{\frac{m_i}{2\pi k_B T_s}}, \qquad (4)$$

where $p_i(T_s)$ is the partial pressure of the ith component above the surface at a surface temperature T_s and m_i is the ith-component particle mass. The coefficient β takes into account the back flux of the plume particles to the surface; for ablation in vacuum it is 0.18 [47, 56].

The main InP ablation products are In atoms and P_2 molecules (see Section 4). The saturated vapour pressure of phosphorus (which is more volatile) exceeds that of indium [57]; therefore, the surface of the initially stoichiometric target is enriched with indium during irradiation, and the total flux of P_2 molecules from the surface decreases. An irradiation for a sufficiently long time leads to establishment of steady-state conditions of congruent vaporisation (see Subsection 4.3), when $j_{In}/m_{In} = 2j_{P_2}/m_{P_2}$. At the same time, it is known that the saturated vapour pressure of indium is the same above InP and metallic In surfaces [57]. Hence, one would expect the saturated vapour pressure of indium to be the same in the intermediate case of indium-rich InP surface. Then the ablation rate can be written as

$$u(t) = u[T_s(t)] = \frac{1-\beta}{\rho}\left(\frac{m_{In} + m_{P_2}/2}{\sqrt{m_{In}}}\right)\sqrt{\frac{1}{2\pi k_B T_s}}\,p_{sat}(T_s), \qquad (5)$$

where p_{sat} is the saturated vapour pressure of indium above the InP surface at a surface temperature T_s. The latter was determined from the Clapeyron–Clausius equation:

$$p_{sat}(T_s) = p_b \exp\left[\frac{L}{k_B}\left(\frac{1}{T_b} - \frac{1}{T_s}\right)\right], \quad (6)$$

where p_b is the reference value of the saturated vapour pressure of In at the boiling temperature T_b.

In the case of developed ablation, radiation screening by the ablation products generally occurs (the laser plasma partially absorbs the radiation) [35, 47, 50, 51]. Under the conditions considered here this effect can be relatively easily taken into account within the model described in [50]. According to [50], the radiation intensity $I(t)$ on the target surface in (1) can be written as

$$I(t) = I_0(t) \exp[-\Lambda(t)], \quad (7)$$

where $I_0(t)$ is the incident radiation intensity and $\Lambda(t)$ is the total optical thickness of the plasma, which has the form

$$\Lambda(t) = a\Delta z(t) + bE_{abs}(t) \quad (8)$$

for moderate radiation intensities. Here, $\Delta z(t)$ is the current ablation depth and

$$E_{abs}(t) = \int_0^t I_0(t')\{1 - \exp[-\Lambda(t')]\}\,dt'$$

is the radiation energy absorbed in the plasma by the instant t. The coefficients a and b are considered as free parameters and chosen proceeding from the best coincidence with the experimental data on the ablation depth.

We theoretically analysed the ablation of indium phosphide by laser pulses with $\lambda = 532$ nm, based on Eqns (1)–(8). The calculation was performed for the real (Gaussian) profile of a 7-ns laser pulse and the following InP parameters: $L = 233$ kJ mol^{-1}, $T_b = 1203$ K, $p_b = 1$ Pa [57], $\alpha_b = 9.5 \times 10^4$ cm^{-1}, and $R = 0.325$ [58], using the temperature dependences $\lambda_T(T)$ [59] and $c(T)$ [60]. It was taken into account that the real laser beam has a Gaussian intensity distribution in the cross section. The solution of Eqn (1) for a constant laser fluence was used to find the local mass $\Delta m = \rho\Delta z$ vaporised from an annular surface area of width Δr within the irradiated spot, where the given intensity is implemented. Then the total removed mass M_0 and effective ablation depth $Z_0 = M_0/(S\rho)$ (S is the spot area) were determined by numerical integration over the spot area.

The results of the calculation within the thermal model are shown in Fig. 2. Disregarding the absorption in the plasma [curve (*2*)], the model adequately describes the experiment only in a relatively narrow range of laser fluences $F_0 \approx 120$–220 mJ cm^{-2}. The target melting threshold corresponds to 97 mJ cm^{-2} (is shown by an arrow in Fig. 2). Note that no fitting parameters were used in this calculation. At $F_0 > 220$ mJ cm^{-2} curve (*2*) is much above the experimental values, which tend to saturate at $F_0 \approx 300$ mJ cm^{-2} due to the screening effect. A calculation with allowance for the absorption in the plasma [with the coefficients $a = 1.5 \times 10^4$ cm^{-1} and $b = 30$ cm^2 J^{-1} from Eqn (8)] allowed us to describe the experimental data in the entire range of laser fluences above the melting threshold [the branch of curve (*3*) for $F_0 > 120$ mJ cm^{-2}]. Note that the found a and b values are in good agreement with the estimates given by the Unsold–Kramers formula for the absorption coefficient in equilibrium plasma [50, 61]. For a plasma temperature of 15000 K (estimate from the TOF distributions of indium atoms, see Section 5) this formula yields $a = 1.3 \times 10^4$ cm^{-1} and $b = 22.4$ cm^2 J^{-1}. Obviously, the surface temperature is much lower. Figure 3 shows the calculated dependence of the maximum surface temperature on F_0.

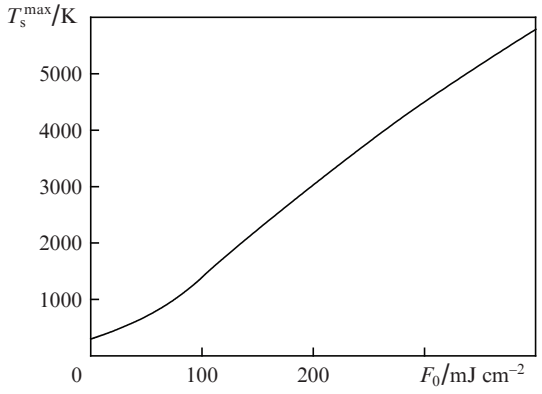

Figure 3. Calculated dependence of the maximum temperature T_s^{max} of the InP surface irradiated by 532-nm laser pulses.

At the same time, at low laser fluences the observed vaporisation rate cannot be described within the thermal mechanism. At $F_0 < 100$ mJ cm^{-2} the experimental values exceed the results of the calculation within the thermal model by one-to-two orders of magnitude (Fig. 2). Obviously, effective nonthermal emission of particles from the InP surface occurs when the irradiated surface temperature is below the melting point. The effect of nonthermal laser desorption from the semiconductor surface is well-known; it is observed at photon energies both higher and lower than the band gap [62–64]. However, the mechanisms of this effect are still insufficiently clear. The nonthermal emission of atoms and ions has been explained in terms of such effects as the localisation of electronic excitation at defects [64, 65], capture of laser-induced carriers (electrons and holes) by surface atoms [63], two-hole localisation [66], surface charging and Coulomb explosion [46, 67], and recombination of electron–hole pairs [68]. The results obtained in this study will be analysed within the Strekalov model [68], which was successfully used to describe the nonthermal emission from semiconductors irradiated with picosecond laser pulses [69].

According to Strekalov, the physical mechanism of nonequilibrium vaporisation from a cold semiconductor surface implies transfer of the nonradiative recombination energy of an electron–hole pair, generated under irradiation, to a surface atom. As a result, the threshold conditions of sublimation change, and its probability sharply increases. The nonequilibrium vaporisation rate, according to [68], has the form

$$J_S = \frac{256\pi^{5/2}}{9\varepsilon_0^2 \hbar k_B T} N n_{e\text{-}h}^{4/3}(t) \sqrt{\frac{E_b - E_g}{k_B T}}\, e^4 a_{lat}^2 \exp\left(-\frac{E_b - E_g}{k_B T}\right), \quad (9)$$

where N is the surface atomic density, $n_{e\text{-}h}(t)$ is the carrier concentration on the irradiated surface, ε_0 is the permittivity, a_{lat} is the lattice constant (5.87 Å for InP), E_b is the atom–surface binding energy, E_g is the band gap (1.35 eV at $T = 300$ K), and

e is the elementary charge. The E_b value for an indium-rich InP surface is unknown; it was used as a free model parameter, whose value was determined from the best agreement between the results of the calculation from formula (9) and the experimental data on the vaporisation depth. Obviously, the E_b value should be between the enthalpy of the InP(s) → In(g) + $^1/_2$P$_2$(g) (4.0 eV [70]) and the enthalpy of indium sublimation above the InP surface (2.4 eV [57]). Thus, for the conditions under consideration we have E_b = 2.75 eV.

To calculate the vaporisation rate from formula (9), one must know the laser-induced nonequilibrium concentrations of carriers (electrons and holes), $n_{e\text{-}h}(t)$, in the semiconductor. The $n_{e\text{-}h}(t)$ dependence was calculated according to the model [71], based on solving the one-dimensional time-dependent continuity equation, taking into account the generation of carriers in the single-photon process of radiation absorption and their annihilation as a result of recombination:

$$\frac{\partial n_c}{\partial t} - u(t)\frac{\partial n_c}{\partial z} = \frac{\partial}{\partial z}\left[D_a(z,T)\frac{\partial n_c}{\partial z}\right]$$

$$+ a_b\frac{I(t)}{\hbar\omega} - \frac{n_c - n_0}{\tau_{Aug}} - \frac{n_c - n_0}{\tau_{rad}}, \qquad (10)$$

where n_c is the carrier concentration (the electron and hole concentrations were assumed to be equal), D_a is the carrier ambipolar diffusion coefficient, $\hbar\omega$ is the photon energy (2.34 eV), and n_0 is the equilibrium carrier concentration at the lattice temperature. In comparison with the equations of model [71], Eqn (10) takes into account not only the Auger recombination but also the radiative recombination of carriers [46]. The corresponding lifetimes τ_{Aug} and τ_{rad} were taken from [2, 58]. The coefficient D_a was calculated using the Einstein equation, which included the temperature dependences for the carrier mobilities from [2]. When calculating the carrier concentration the lattice temperature T was taken from the solution to the heat-conduction equation. The calculation was performed for temperatures below the melting point, because InP is metallised during melting [72], resulting in complete recombination of electron–hole pairs.

The results of simulating the generation of nonequilibrium carriers in InP under laser pulses with λ = 532 nm are shown in Fig. 4. The time evolution of the carrier concentration in the surface layer at a laser fluence of 60 mJ cm^{-2} is presented in Fig. 4a. The maximum value $n_{e\text{-}h} \simeq 2\times10^{19}$ cm^{-3} is in good agreement with Strekalov's estimation [68] of the carrier concentration at which semiconductors should undergo intense nonequilibrium vaporisation. Note that this $n_{e\text{-}h}$ value is two orders of magnitude lower than the critical plasma density (4×10^{21} cm^{-3} [61]); therefore, the radiation is not screened by carriers. The time dependence $n_{e\text{-}h}(t)$ practically repeats the laser pulse profile (Fig. 4a), that is explained by the high recombination rate of electron–hole pairs ($\tau_{rad} \sim 160$ ps for $n_{e\text{-}h} \sim 10^{19}$ cm^{-3} [2]). For comparison Fig. 4 shows also the time profile of the surface temperature T_s, whose maximum is ~5 ns behind the laser pulse peak. This delay in surface heating is related to the heat outflow into the target bulk due to the thermal conductivity [73]. The laser fluence dependences of the maximum $n_{e\text{-}h}$ and T_s values for the regimes without target melting are shown in Fig. 4b.

The Strekalov model made it possible to explain the observed high vaporisation rates of InP at low radiation

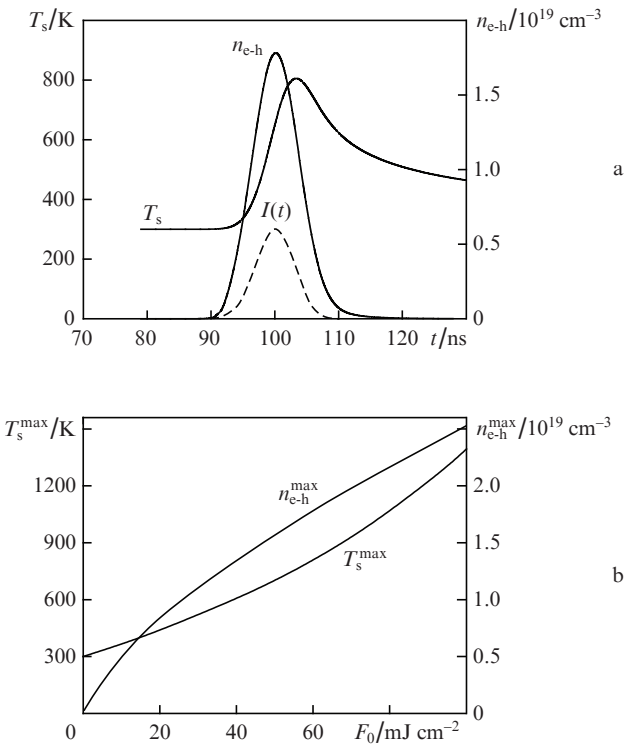

Figure 4. Time dependences of the nonequilibrium carrier concentration $n_{e\text{-}h}$ and temperature T_s of the InP surface for a laser fluence of 60 mJ cm^{-2} (a) and the fluence dependences of the maximum $n_{e\text{-}h}$ and T_s values (b). The dashed curve is the profile of a 532-nm laser pulse (in the calculations the pulse peak corresponded to the instant t = 100 ns).

intensities. The vaporisation depth calculated from formula (9) for the binding energy E_b = 2.75 eV is shown in Fig. 2 [curve (*1*)]. The maximum depth of the nonthermal emission is realised near the melting point and amounts to ~ 0.01 ML. Apparently, this effect can be used for precise treatment and structurisation of semiconductor surfaces by low-intensity nanosecond laser pulses. The total rate of thermal and nonthermal vaporisation is shown in Fig. 2 by curve (*3*). It can be seen that the combined model quite adequately describes the experimental data in the entire range of F_0 values.

Thus, the ablation of indium phosphide by 532-nm laser pulses of moderate or high intensity (above the melting threshold) is described well by the thermal mechanism. For well-developed ablation ($F_0 > 200$ mJ cm^{-2}) one must take into account the radiation screening by the ablation plasma. Effective nonthermal emission of particles from the surface occurs at low irradiation intensities (below the melting threshold); it can be explained within the Strekalov model [68] by the recombination of laser-induced electron–hole pairs. Note that intense nonthermal emission of particles from the surface irradiated with low-intensity laser pulses is apparently typical of binary semiconductors. For example, in the case of ablation of cadmium telluride by KrF laser pulses the measured vaporisation depth significantly exceeds the value calculated within the thermal model for $F_0 < 60$ mJ cm^{-2} [53].

4. Composition of ablation products

Figure 5 shows typical mass spectra of the main neutral ZnO and InP ablation products. Zn atoms and O_2 molecules are the main particles for ZnO ablation. The content of atomic

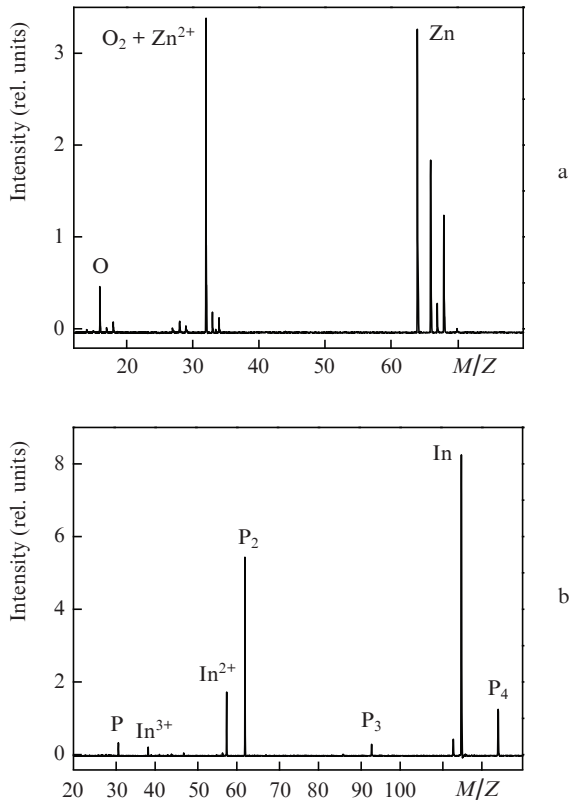

Figure 5. Typical mass spectra of the main neutral ablation products of (a) ZnO and (b) InP by 532-nm laser pulses at laser fluences F_0 = 1.5 J cm^{-2} (a) and 250 mJ cm^{-2} (b). The particles were ionised by electron impact.

oxygen is much lower. Singly charged particles (mainly Zn^+ ions and, in a smaller amount, Zn^{2+} ions) are observed in the plume at laser fluences above ~0.7 J cm^{-2}. An estimation of the ion fraction (with due regard to the mass-spectrometer sensitivity to neutral and charged particles) indicates that the degree of plume ionisation does not exceed 2% in the entire range of F_0 values under study. In the case of InP ablation the main products are neutral In and P_2. In addition, P atoms and P_3 and P_4 molecules are present in rather large amounts (Fig. 5b). The charged plume components are also mainly metal ions: In^+ and In_2^+. P^+ ions were also observed at high laser fluences. Due to the low ionisation potential of indium (5.8 eV), the ionisation degree of the InP plume exceeded that for the ZnO ablation and reached ~10% at F_0 ~ 1 J cm^{-2}. Accordingly, the plasma formation thresholds were fairly low: ~150 mJ cm^{-2} for 532-nm pulses, ~300 mJ cm^{-2} for 1064-nm pulses, and ~100 mJ cm^{-2} for 800-nm femtosecond pulses.

Under certain irradiation conditions neutral and charged clusters of different stoichiometry were observed in the ablation products. The results of studying the cluster formation during ZnO and InP laser ablation are discussed below.

4.1. Cluster formation during laser ablation of zinc oxide

In the case of ZnO laser ablation Zn_nO_m clusters of different composition, having a wide size distribution, were detected in the ablation products in the entire wavelength range under study (from UV to IR). The clusters were observed in narrow ranges of laser fluence: approximately 0.5–1, 1–3, and 2–4 J cm^{-2} for λ = 193, 532, and 1064 nm, respectively. Thus, the F_0 value that is optimal for cluster formation decreases with decreasing radiation wavelength.

Figure 6 shows a typical mass spectrum of particles produced during ZnO ablation by UV laser pulses (λ = 193 nm), for which the photon energy (6.4 eV) is higher than the band gap (3.37 eV). The main clusters are enriched with zinc. Depending on the ratio of the numbers of metal and oxygen atoms, the clusters can be divided into three series: $Zn_nO_{n-k}^+$ with k = 1, 2, and 3. The series with one missing oxygen atom, characterised by a monotonically decreasing cluster size distribution, had the highest concentration. The series with k = 3 appears to dominate over that with k = 2. Stoichiometric clusters $(ZnO)_n^+$ were observed in very small amounts, with n = 2, 3, and 6–9. When varying the delay time τ, it was found that all clusters have approximately the same velocity (~1.4 km s^{-1}) in the plume, despite the significant difference in their masses. This fact indicates that clusters are formed as a result of particle aggregation in the expanding plume (as in supersonic gas jets [74, 75]) rather than emitted from the target surface, when one would expect equal kinetic energies of clusters [20, 45].

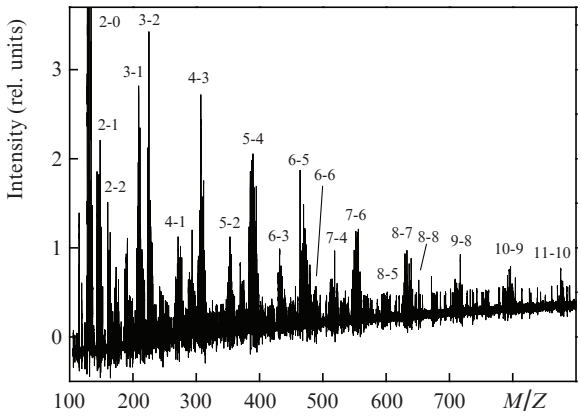

Figure 6. Mass spectrum of charged $Zn_nO_m^+$ clusters in the products of ZnO ablation by 193-nm laser pulses at a laser fluence F_0 = 0.8 J cm^{-2} and delay time τ = 42 μs (corresponds to the maximum cluster yield). The paired numbers (n–m) above the peaks indicate the numbers of Zn and O atoms per cluster. The spectrum was obtained by averaging over the first 25 laser pulses irradiating a fresh ZnO surface.

In the case of ZnO ablation by UV laser pulses, intense cluster formation with a distribution similar to that in Fig. 6 is observed only for fresh target surfaces, irradiated with no more than 50 pulses. At longer irradiation times the cluster yield sharply decreases. This fact, as well as the nonstoichiometry of the clusters formed, is explained by the enrichment of the ZnO surface with zinc under irradiation with λ = 193 nm (100 pulses are sufficient for enrichment up to ~80% [37]). To obtain stoichiometric clusters under these conditions, one must use an oxygen-containing background gas [21, 25]. Note that purely metallic Zn_n clusters are not formed even with excess zinc in the laser plume.

The situation is completely different in the case of ZnO ablation by visible and IR laser pulses, when the photon energies are lower than the band gap. Clusters of various composition, especially stoichiometric ones, are effectively formed under these conditions. Figure 7 shows the mass spectrum of $Zn_nO_m^+$ cluster cations in the ablation products of ZnO irradiated with 1064-nm pulses; this wavelength provides the most efficient cluster formation [under optimal conditions (F_0 =

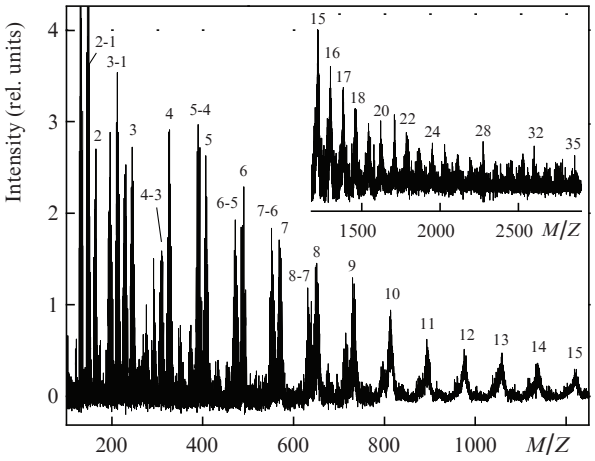

Figure 7. Mass spectrum of charged $Zn_nO_m^+$ clusters in the products of ZnO ablation by 1064-nm laser pulses at a laser fluence $F_0 = 3$ J cm^{-2} and delay time $\tau = 40$ μs. The n–m labels are as in Fig. 6. Single numbers above peaks indicate the number n of atoms in stoichiometric $(ZnO)_n$ clusters.

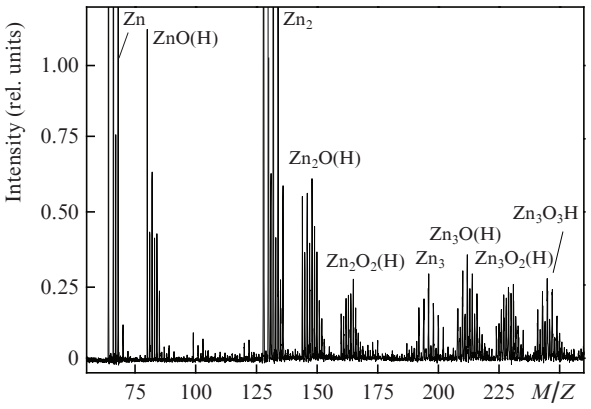

Figure 8. Mass spectrum of small charged $Zn_nO_m^+$ clusters. The ablation and detection conditions are as in Fig. 7. Peaks corresponding to a mixture of pure and hydrogenated zinc oxide clusters are labeled as $Zn_nO_m(H)$.

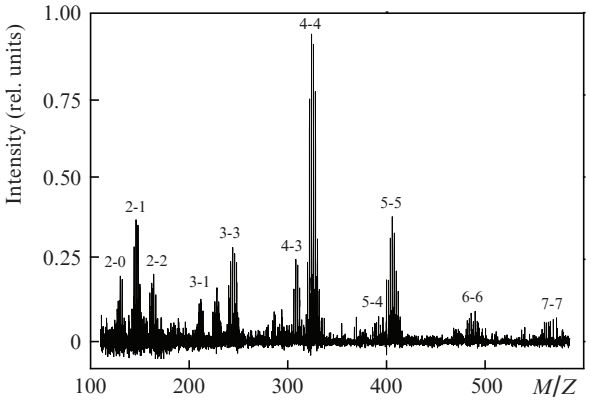

Figure 9. Mass spectrum of neutral Zn_nO_m clusters in the products of ZnO ablation by 1064-nm laser pulses (electron-impact ionisation). The ablation conditions and designations of peaks are as in Fig. 7.

2–4 J cm^{-2}) the fraction of cluster ions reaches 10% of the total number of charged particles in the plume]. Note that a long-term irradiation of the same point of the target surface does not significantly reduce the cluster yield. As in the case of UV laser ablation, clusters of all sizes have the same average velocity (~1.5 km s^{-1}), that is indicative of their condensation nature.

The cluster size distribution monotonically decreases, without any pronounced 'magic' particles, whereas, the composition of clusters depends on their size (n value) (Fig. 7). The smallest clusters ($n = 2, 3$) are mainly off-stoichiometric ($n > m$). Small clusters ($n = 4$–9) yield a double peak, which corresponds to $Zn_nO_n^+$ and $Zn_nO_{n-}^+$ particles with approximately the same concentration. Medium-size and large clusters ($n > 9$) are mainly stoichiometric. The largest experimentally observed cluster has $n = 35$; however, taking into account that the detection efficiency of mass spectrometer with microchannel plates sharply decreases for large clusters [76, 77], one might expect heavier particles to be present in the plume and the real distribution to be shifted to larger sizes. Distributions similar to that in Fig. 7 were obtained by us for ZnO ablation by 532-nm laser pulses and by Kukreja et al. [42] for ablation with 337-nm pulses. At the same time, only few weak cluster signals were detected during ZnO ablation by IR (1064 nm) pulses in [43]; this is apparently due to the very high laser fluence (7.7 J cm^{-2}) used in [43].

A detailed analysis of the mass spectrum in Fig. 7 shows that stoichiometric charged clusters $(ZnO)_n^+$ have a high reactivity toward hydrogen, element that is likely to be present in trace amounts in the target. The reactivity of $Zn_nO_m^+$ clusters decreases with a decrease in the number m of oxygen atoms, as can be seen in Fig. 8. For example, Zn_3^+ trimers do not interact with hydrogen. Oxygen-deficient pure (Zn_3O^+ and $Zn_3O_2^+$) and the corresponding hydrogenated (Zn_3OH^+ and $Zn_3O_2H^+$) clusters have approximately the same concentrations (the mass spectrum contains two almost identical isotopic distributions shifted by 1 amu). At $n = m$, $Zn_3O_3H^+$ particles dominate over pure stoichiometric clusters (Fig. 8); however, with an increase in n the reactivity of $(ZnO)_n$ clusters decreases [27].

Figure 9 shows a typical mass spectrum of neutral clusters, recorded under the same 'optimal' ablation conditions as the spectrum of charged clusters (see Fig. 7). Particles were ionised by electron impact. The neutral clusters are mainly stoichiometric and highly stable to hydrogenation (hydrogen-containing neutral clusters were not observed). The most striking feature of the distribution obtained is the dominance of the $(ZnO)_4$ tetramer. This is fairly unexpected, because the quantum-mechanical calculations of the structures of small neutral zinc oxide clusters [78, 79] did not predict any peculiar tetramer stability. We believe its manifestation in the spectrum as a 'magic' cluster to be due to the electron-impact caused fragmentation of larger clusters. This suggestion is favoured by the fact that the tetramer is one of the building blocks of zinc oxide clusters [79]. We tried to detect neutral clusters in the ZnO ablation products using photoionisation by 193-nm laser radiation instead of electron impact but could not detect particles larger than dimers. Such an efficient photofragmentation indicates that the cluster ionisation potential E_i exceeds the photon energy (6.4 eV), and two-photon ionisation occurs, which is characterised by a high fragmentation probability [80]. Indeed, according to calculations [78], the potential E_i of $(ZnO)_n$ clusters with $n = 10$–16 is about 7.7 eV. It is of interest to investigate neutral zinc oxide clusters (which are likely to be present in the plume in significant amounts, including large-size clusters, under the given ablation conditions) using 'soft' single-photon ionisation, for example, with F_2

laser radiation (photon energy 7.9 eV). We plan to perform such experiments in the nearest future.

4.2. Cluster formation during laser ablation of indium phosphide

As in the case of ZnO, indium phosphide clusters were detected only in relatively narrow ranges of laser fluences: 200–400 and 400–700 mJ cm^{-2} for λ = 532 and 1064 nm, respectively. For femtosecond IR pulses, which provided especially efficient cluster formation, they were observed in the entire range of F_0 values under study, starting from the ablation threshold (~100 mJ cm^{-2}). As for ZnO, the cluster formation conditions depend strongly on how the photon energy is related to the band gap (i.e., exceeds it or not). However, in contrast to zinc oxide clusters, the clusters in the ablation products of InP are significantly enriched with metal in all cases.

In the case of ablation of indium phosphide by 532-nm laser pulses charged clusters were observed only for a fresh InP surface, irradiated by no more than 20 pulses. An analysis of the composition of the ablation products after each pulse showed that the cluster yield reaches a maximum after the third and fourth pulses and then sharply decreases. The first two pulses serve to prepare the surface for cluster emission and remove surface impurities. Figure 10 shows the mass spectrum of ions recorded after the fourth pulse. In contrast to the smooth distributions of zinc oxide cluster cations (Figs 6, 7), there are only four 'magic' $In_nP_m^+$ clusters (n = 4–6, m = 1–3) in the mass spectrum. It is noteworthy that specifically these particles were previously observed in the analysis of the neutral ablation products of InP irradiated by laser pulses in a background gas [24]. Here, we performed experiments without a background gas, and did not detect any neutral clusters during InP ablation by visible light.

The situation is quite different for InP ablation by IR laser pulses (both nanosecond and femtosecond) with $\hbar\omega < E_g$; here, both neutral and charged clusters are present in significant amounts in the plume. Similarly to the ablation of ZnO by visible and IR laser pulses, now clusters are produced not only with a fresh surface but also with the target surface subjected to long-term irradiation. Figure 11 shows a mass spectrum of the charged clusters obtained under multiple (more than 1000 pulses) irradiation of InP by 800-nm femtosecond laser pulses (case of the most efficient cluster formation). All

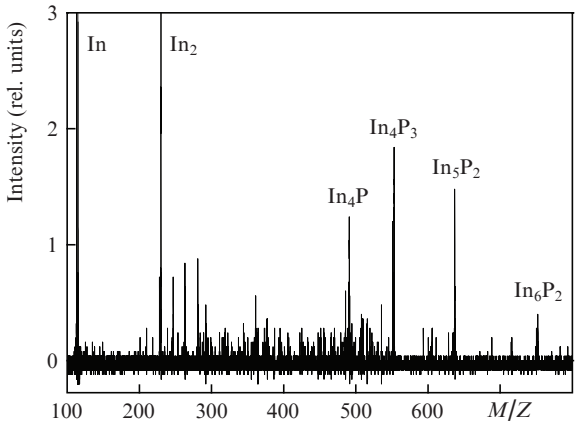

Figure 10. Mass spectrum of charged $In_nP_m^+$ clusters in the products of InP ablation by 532-nm laser radiation at a laser fluence F_0 = 280 mJ cm^{-2}. The spectrum was recorded after the fourth pulse irradiating a fresh InP surface.

$In_nP_m^+$ clusters are strongly nonstoichiometric, and even the largest of them contain no more than three phosphorus atoms. The same cations that were observed during ablation by 532-nm laser pulses (Fig. 10) are dominant in the mass spectrum. Depending on the number of indium and phosphorus atoms, $In_nP_m^+$ clusters can be divided into two main groups: In_nP^+ and $In_nP_2^+$; note that the sum $n + m$ is an odd number (except for the In_6P_2 cluster). As in the case of zinc oxide clusters, all $In_nP_m^+$ clusters have approximately the same velocities (~2 km s^{-1}) in the laser plume, which suggests their formation through condensation in the gas phase. The use of 1064-nm nanosecond pulses for ablation leads to generation of clusters with a similar distribution (Fig. 11) but with a lower yield. The latter is not surprising because femtosecond laser ablation provides generally more favourable (in comparison with nanosecond ablation) conditions for particle aggregation in the gas phase [20, 81] due to the absence of radiation absorption in the plasma and sharp 'forward' directionality of the laser plume (which increases the number of particle collisions during plume expansion).

A typical mass spectrum of neutral clusters for the ablation of InP by IR laser pulses is shown in Fig. 12. In these experiments particles were ionised by an ArF laser, with a photon

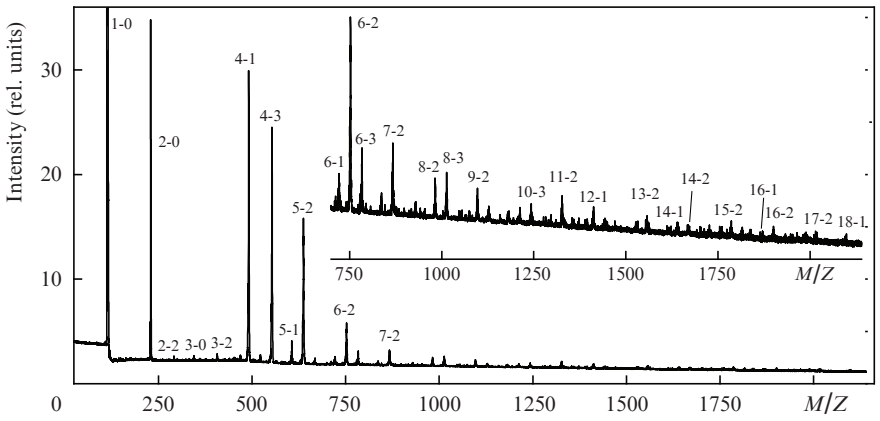

Figure 11. Mass spectrum of charged $In_nP_m^+$ clusters in the products of InP ablation by femtosecond 800-nm laser pulses at a laser fluence F_0 = 260 mJ cm^{-2}. The paired numbers above peaks indicate n and m values.

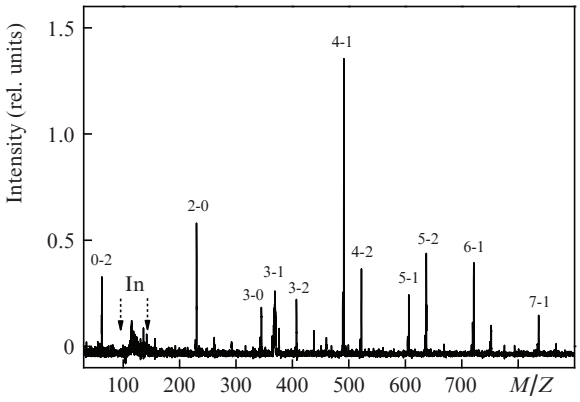

Figure 12. Mass spectrum of neutral In_nP_m clusters in the products of InP laser ablation (λ = 1064 nm, F_0 = 500 mJ cm^{-2}). Ionisation was performed by unfocused ArF laser radiation with an energy density of ~20 mJ cm^{-2}. The detector was blocked during the arrival of the dominant In^+ ions with a filter (the blocked interval is shown by the dashed arrows).

energy (6.4 eV) exceeding the ionisation potential E_i of the In_nP_m cluster (at least for $n > 3$ [24]); therefore, it can be assumed that there is no significant fragmentation of clusters during ionisation, and the distribution observed corresponds to the true one. Like $In_nP_m^+$ cluster cations, neutral particles are significantly enriched with indium. Comparing the distributions in Figs 11 and 12, one can see that the number of phosphorus atoms in neutral clusters is generally smaller by one than in cations with the same n. Note that In_4P and In_5P_2 clusters manifest themselves as 'magic' in both distributions. The fact that all In_nP_m clusters in the laser plume are significantly enriched with indium is explained (see below) by the incongruent InP vaporisation and the character of subsequent expansion of the plume particles.

4.3. Effect of the number of laser pulses on the composition of the ablation products

To trace the evolution of laser-induced vaporisation of the ZnO and InP targets, we performed mass-spectrometric measurements of the yields of the main neutral ablation products for these materials under successive irradiation of the same point of initially fresh surface by single laser pulses. The laser fluence was maintained constant, and the delay time τ corresponded to the largest signal of particles (maximum in the TOF distributions). Figure 13a shows the results of these measurements for Zn atoms and O_2 molecules in the products of ZnO ablation by 1064-nm laser pulses with F_0 = 3 J cm^{-2} (i.e., under the most favourable conditions for cluster generation; see Subsection 4.1). First, after the first few pulses, the particle yield decreases to a minimum; then increases again; and after ~1000 pulses reaches a quasi-steady-state value, without any further changes. Similar dependences were obtained for smaller F_0 values (in this case a larger number of pulses was necessary to reach the steady-state level) and for 532-nm pulses.

This nonmonotonic dependence is likely to be caused by a complex modification of the ZnO surface during irradiation and the change in its optical properties, in particular, due to the generation of oxygen vacancies [21]. The more important fact (in the context of laser synthesis of clusters) is that the ratio of the zinc and oxygen yields remains constant (~1 within the experimental error). This means that under these

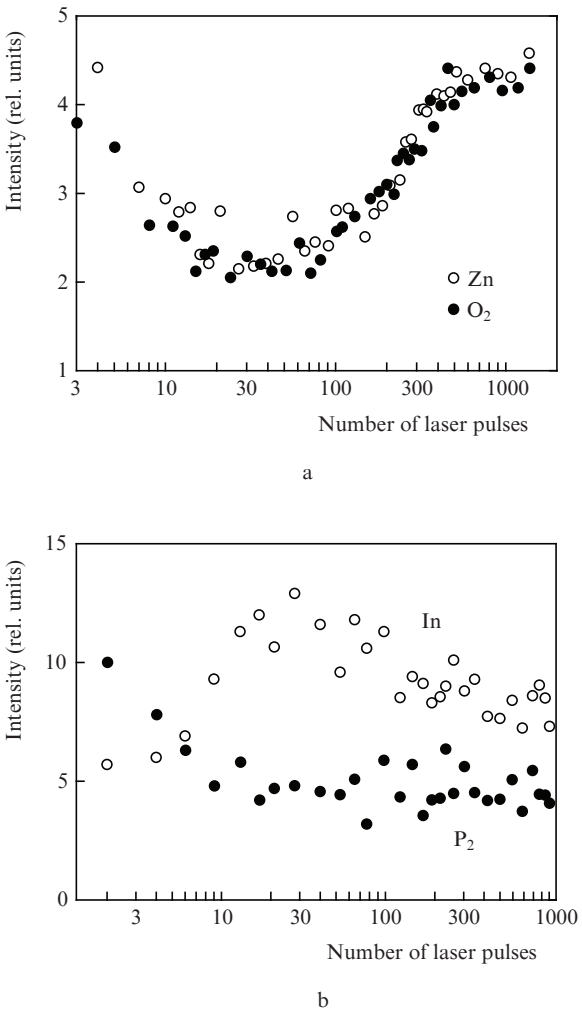

Figure 13. Dependences of the yields of the main neutral ablation products of ZnO (a) and InP (b) on the number of successive 1064-nm laser pulses with the delay time τ = 30 μs and laser fluences F_0 = 3 (a) and 0.5 J cm^{-2} (b).

conditions the laser vaporisation of ZnO occurs congruently, without a change in the target surface composition, as during conventional thermal heating. At the same time, incongruent vaporisation obviously occurred in the case of ZnO irradiation by 193-nm pulses, when the surface was enriched with zinc [37], and nonstoichiometric clusters were formed (see Subsection 4.1).

The composition of the InP ablation products evolves during target irradiation quite differently. The dependences of the yields of In atoms and P_2 molecules on the number of pulses under optimal (for cluster formation) ablation conditions (λ = 1064 nm, F_0 = 500 mJ cm^{-2}) are shown in Fig. 13b. After the irradiation of a fresh surface by the first few pulses the signal of more volatile phosphorus significantly exceeds the indium signal. Further pulsed irradiation leads to a sharp decrease in the phosphorus yield and, vice versa, to an increase in the absolute indium yield. After several hundreds of pulses both signals reach quasi-steady-state values (which are larger for indium). Similar dependences were observed by us under irradiation with λ = 532 nm and previously for irradiation with λ = 337 nm in [36]. A natural explanation of this effect is that, as upon thermal heating, the vaporisation is incongruent and the irradiated target loses an unproportionally large

amount of phosphorus. Indeed, a study of the InP surface after irradiation by 532-nm pulses showed that it is enriched with indium when the radiation energy density exceeds some threshold value [82]. However, it is important to note the following. The tendency of the aforementioned dependences to quasi-steady-state values after a fairly large number of laser pulses (Fig. 13b) indicates that on the whole (integrally) the vaporisation becomes congruent, despite the excess indium on the surface. This is possible in the case of phosphorus and indium vaporisation on different time scales. Below we will show that this condition is indeed realised in the multipulse InP ablation.

The experimental results discussed in this section indicate that the cluster formation during laser ablation of ZnO and InP semiconductors depends strongly on the relation between the light photon energy $\hbar\omega$ and the semiconductor band gap E_g. At $\hbar\omega > E_g$ only charged clusters are observed, and the efficiency of their formation rapidly decreases during the target irradiation. On the contrary, at $\hbar\omega < E_g$, charged and neutral clusters are present in the ablation products in significant amounts, and a long-term target irradiation does not lead to a significant decrease in their abundance. Obviously, additional detailed study must be performed to explain these facts. We can suggest that this behaviour is caused by the significant difference in the semiconductor optical properties for the two cases under consideration (in particular, in the absorption coefficients). At $\hbar\omega > E_g$ the laser energy is absorbed in a thin surface skin layer; therefore, it is difficult to simultaneously satisfy the two conditions that are necessary for the particle aggregation in the plume: a sufficiently high density of particles (i.e., large ablation depth) and their relatively low temperature, at which a high degree of vapour supersaturation can be implemented in the plume [14, 20, 83, 84]. In addition, in this case ablation is generally determined to a great extent by nonthermal (electronic) mechanisms [35], which lead to a direct break of atomic bonds on the surface and effective removal of a more volatile component (including such materials as ZnO, which evapourate congruently upon thermal heating). For low-energy photons ($\hbar\omega < E_g$) the absorption coefficient is small, and the radiation penetrates deep into the target. Under these conditions, it is more likely to find an irradiation regime in which a fairly large amount of material vaporises at not very high temperature. Such favourable (for cluster formation) regimes are implemented, as shown in this study, only in narrow ranges of laser fluences.

5. Expansion dynamics of ablation products

To analyse the processes of laser vaporisation of binary semiconductors and cluster formation, we studied the expansion dynamics of the main ZnO and InP ablation products by varying the delay time τ between the laser and ionisation pulses. Figure 14a shows the TOF distributions of neutral Zn and O_2 particles for the optimal conditions of ZnO ablation (λ = 1064 nm, F_0 = 3 J cm^{-2}), which correspond to the highest cluster yield (see Figs. 7 and 9). It can be seen that zinc atoms and oxygen molecules have the same average velocity and expand jointly, despite the significant difference in their masses. This indicates that the hydrodynamic (collisional) stage of plume expansion is fairly long [45], which facilitates aggregation. The collisions of particles of different type are equiprobable under these conditions. Hence, clusters can be self-assembled into the most preferred stable structures, which are most likely stoichiometric for zinc oxide.

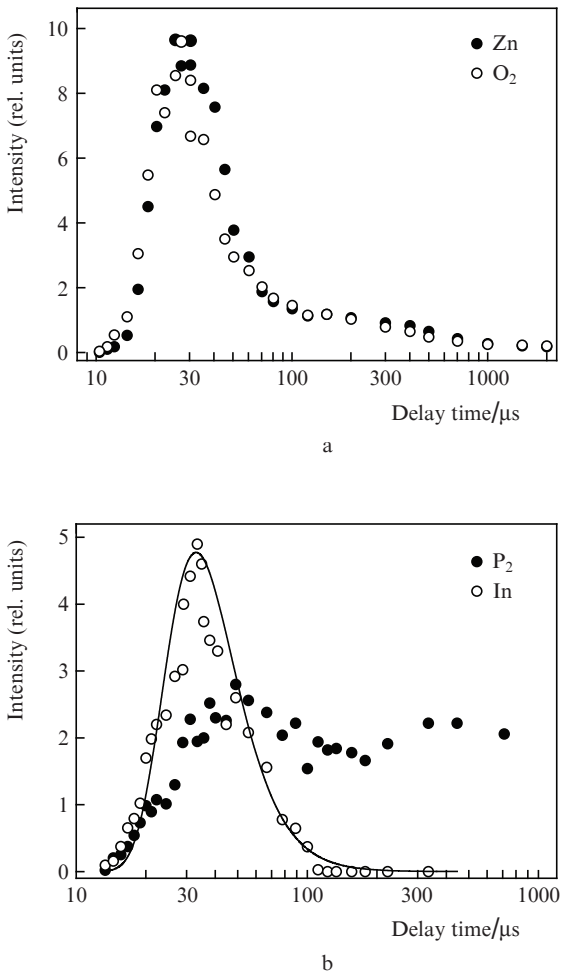

Figure 14. Time-of-flight distributions of the main neutral products of ablation of ZnO (a) and InP (b) by 1064-nm laser radiation at F_0 = 3 (a) and 0.5 J cm^{-2} (b). The solid line is an approximation of the data for indium atoms by the Maxwell–Boltzmann distribution with an effective temperature of 15000 K.

The character of plume expansion is quite different for the ablation of indium phosphide. Figure 14b shows the TOF distributions of In atoms and P_2 molecules, obtained for the ablation conditions corresponding to the maximum cluster yield (λ = 1064 nm, F_0 = 500 mJ cm^{-2}; see Fig. 12). The distribution of indium atoms is similar to that observed for Zn and O_2 in the case of ZnO ablation (Fig. 14a): it contains one peak, is rather narrow, and its maximum is at the same value $\tau \approx 30$ μs (the corresponding most probable velocity is ~2 km s^{-1}). An approximation of the TOF distribution of indium by the equilibrium Maxwell–Boltzmann distribution (solid line in Fig. 14b) gives a reasonable effective temperature of particles in the plume: ~15000 K. At the same time, lighter P_2 molecules arrive at the detection point with a significant delay in comparison with indium atoms. In the TOF distribution of phosphorus molecules this effect manifests itself as a slow tail (Fig. 14b). With an increase in the laser fluence to 700 mJ cm^{-2} or higher these slow molecules become dominant. Similar TOF distributions with a delayed tail were obtained for other phosphorus particles (P, P_3, and P_4) in the case of InP ablation by 532- and 1064-nm laser pulses. This feature of expansion of phosphorus particles can be explained by the congruent (integrally throughout a pulse) InP vaporisation under multipulse laser irradiation (see Section 4). Indeed, the target surface is

enriched with indium in this case, and, when the ablation has a thermal character, most In atoms evapourate during the pulse, when the surface temperature is maximum (see Section 3). The irradiation-induced heating of the target activates diffusion in the surface layer and partially compensates for the deficit of the more volatile component on the surface [52, 53]. The phosphorus particles diffused from the target bulk to the surface evapourate for a fairly long time upon target cooling (at least to the surface temperature $T_s \sim 600$ K [31]), and this process manifests itself as a tail in the distribution of P_2 molecules in Fig. 14b. The higher the laser fluence, the stronger the surface enrichment with indium and, therefore, the larger the number of phosphorus particles evapourated with a delay. As a result, vaporisation stoichiometry is implemented under multipulse irradiation of InP. Due to the time delay between the processes of indium and phosphorus vaporisation during laser ablation of InP and the different expansion velocities of In and P_2 particles, these particles are unlikely to collide during their flight, whereas the probability of indium–indium collisions is high. This circumstance explains why the clusters observed in the case of InP ablation are significantly enriched with indium.

The experimental results reported here indicate that the character of laser vaporisation of binary semiconductors (congruent or incongruent) is in many respects the same as for conventional thermal heating. Thus, the composition of particles in the ablation products (their stoichiometry or off-stoichiometry) can be predicted based on the thermodynamic properties of the evapourated materials. The question why some compound semiconductors (for example, ZnO) evapourate congruently, while the others (such as InP) evapourate incongruently, is beyond the scope of this study and requires a separate consideration. In our opinion, the character of vaporisation is essentially determined by the range of component concentrations in which the material remains thermodynamically stable (or, in other words, by the existence of the homogeneity ranges in the condensed phase for the compound [85]). The wider this range, the larger the deviation from stoichiometry during vaporisation can be. From the physical point of view this apparently means that compounds with a variable composition can be structurally transformed upon heating so as to release the more volatile component. In particular, melting of some binary semiconductors may lead to the formation of clusters and branched chains of like-atoms [86]. Concerning the materials under study, the crystal structure of ZnO is known to be stable only in a very narrow range of component concentrations (deviation from stoichiometry does not exceed 0.1 at% [87]). Therefore, ZnO evapourates congruently. On the contrary, indium phosphide remains stable in a wide range of component concentrations (at least from 0 to 55 at% phosphorus [88]); therefore, its vaporisation is incongruent.

6. Conclusions

We performed a comparative analysis of cluster formation during pulsed laser ablation of two binary semiconductors, ZnO and InP, in vacuum. Nanostructures based on these semiconductors are promising for many applications. Ablation was performed using nanosecond and femtosecond laser pulses in a wide range of wavelengths, from UV to IR. The main attention was paid to the analysis of the ablation mechanisms and study of small clusters in the ablation products (their formation mechanisms and conditions, composition, and reactivity), which serve as nuclei for the growth of larger clusters. It was shown by the example of indium phosphide that for medium and high laser fluences (above the melting threshold) ablation is described well within the thermal model. Effective desorption from the surface was found at low fluences, which cannot be explained in terms of the thermal mechanism. A model of nonthermal particle emission from the semiconductor surface was developed based on the Strekalov mechanism of nonequilibrium vaporisation [68]. Neutral and charged clusters of different stoichiometry were detected in narrow ranges of laser fluences in the ZnO and InP ablation products.

It was established that clusters are formed most efficiently during semiconductor ablation by radiation with a photon energy below the semiconductor band gap. In this case, zinc oxide clusters are mainly stoichiometric, and the size distribution of charged clusters does not contain any preferred sizes. The peak corresponding to the $(ZnO)_4$ tetramer dominates in the mass spectrum of neutral clusters; it is apparently due to the fragmentation of larger neutral clusters under the probe electron beam. On the contrary, all detected In_nP_m clusters (both neutral and charged) are off-stoichiometric and significantly enriched with indium (the number of P atoms per cluster does not exceed three); the 'magic' In_4P cluster has the highest concentration.

It was found that small stoichiometric cluster cations $(ZnO)_n^+$ have high reactivity toward hydrogen. Based on a mass-spectrometric analysis of the evolution of the laser plume composition during irradiation of semiconductors by a sequence of laser pulses and a study of the plume expansion dynamics, it was established that laser ablation of zinc oxide occurs congruently in a wide range of irradiation conditions. Moreover, at certain laser fluences the main ZnO ablation products expand jointly, which facilitates the formation of stoichiometric clusters. On the contrary, ablation of indium phosphide is accompanied by preferred loss of phosphorus from the irradiated surface. The effect of delayed phosphorus vaporisation under multipulse laser irradiation of InP was found. This effect is explained by the activation of phosphorus diffusion to the surface under irradiation. The experimental results obtained indicate that the character of laser ablation of binary semiconductors (congruent or incongruent vaporisation) determines the cluster composition in the ablation products.

Acknowledgements. We are grateful to N.M. Bulgakov and J. Bonse for useful and stimulating discussions. The indium phosphide samples were kindly supplied by J. Bonse.

This work was supported by the Russian Foundation for Basic Research (Grant No. 09-02-91291-CSIC).

References

1. Alferov Zh.I. *Usp. Fiz. Nauk*, **172**, 1068 (2002).
2. Pearsall T.P. (Ed.) *Properties, Processing and Applications of Indium Phosphide* (London: IEE Publishing, 2000).
3. Jagadish C., Pearton S. (Eds) *Zinc Oxide Bulk, Thin Films and Nanostructures* (Oxford–Amsterdam: Elsevier, 2006).
4. Chandrasekhar S. *Solid-State Electron.*, **41**, 1413 (1997).
5. Haug H., Koch S.W. *Quantum Theory of the Optical and Electronic Properties of Semiconductors* (Singapore: World Scientific Publishing, 1994).
6. Morales-Acevado A. *Solar Energy*, **80**, 675 (2006).

7. Zweibel K. *Science*, **328**, 699 (2010).
8. Xu S., Ziegler J., Nann T. *J. Mater. Chem*., **18**, 2653 (2008).
9. Late J.D., Misra P., Singh B.N., Kukreja L.M., Joag D.S., More M.A. *Appl. Phys. A*, **95**, 613 (2009).
10. Özgür Ü., Alivov Y.I., Liu C., Teke A., Reshchikov M.A., Doğan S., Avrutin V., Cho S.-J., Morkoç H. *J. Appl. Phys.*, **98**, 041301 (2005).
11. Huang M.H., Mao S., Feick H., Yan H., Wu Y., Kind H., Weber E., Russo R., Yang P. *Science*, **292**, 1897 (2001).
12. Chelnokov E.V., Bityurin N., Ozerov I., Marine W. *Appl. Phys. Lett*., **89**, 171119 (2006).
13. Johnston R.L. *Atomic and Molecular Clusters* (London: CRC Press, 2002).
14. Smirnov B.M. *Usp. Fiz. Nauk*, **173**, 609 (2003).
15. Makarov G.N. *Usp. Fiz. Nauk*, **176**, 121 (2006).
16. Patrone L., Nelson D., Safarov V.I., Sentis M., Marine W. *J. Appl. Phys.*, **87**, 3829 (2000).
17. Seto T., Orii T., Hirasawa M., Aya N. *Thin Solid Films*, **437**, 230 (2003).
18. Luk'yanchuk B., Marine W. *Appl. Surf. Sci.*, **154-155**, 314 (2000).
19. Anisimov S.I., Luk'yanchuk B.S. *Usp. Fiz. Nauk*, **172**, 301 (2002).
20. Bulgakov A.V., Ozerov I., Marine W. *Appl. Phys. A*, **79**, 1591 (2004).
21. Ozerov I., Nelson D., Bulgakov A.V., Marine W., Sentis M. *Appl. Surf. Sci.*, **212-213**, 349 (2003).
22. Neretina S., Mascher P., Hughes R.A., Braidy N., Gong W.H., Britten J.F., Preston J.S., Sochinskii N.V., Dippo P. *Appl. Phys. Lett*., **89**, 133101 (2006).
23. Bonse J., Munz M., Sturm H. *J. Appl. Phys.*, **97**, 013538 (2005).
24. Kolenbrander K.D., Mandich M.L. *Phys. Rev. Lett.*, **65**, 2169 (1990).
25. Ozerov I., Bulgakov A.V., Nelson D.K., Castell R., Marine W. *Appl. Surf. Sci.*, **247**, 1 (2005).
26. Jadraque M., Domingo C., Martin M. *J. Appl. Phys.*, **104**, 024306 (2008).
27. Bulgakov A.V., Evtushenko A.B., Shukhov Y.G., Ozerov I., Marine W. *Appl. Phys. A*, **101**, 585 (2010).
28. Bulgakov A.V., Evtushenko A.B., Shukhov Y.G., Ozerov I., Marine W. *AIP Conf. Proc.*, **1278**, 78 (2010).
29. L'vov B.V. *Termorazlozhenie tverdykh i zhidkikh veshchestv* (Thermal Decomposition of Solid and Liquid Materials) (St. Petersburg: Izd-vo Politekh. Univ., 2006).
30. Anthrop D.F., Searcy A.W. *J. Phys. Chem.*, **68**, 2335 (1964).
31. Farrow R.F.C. *J. Phys. D: Appl. Phys.*, **7**, 2436 (1974).
32. Fang R., Brebrick R.F. *J. Phys. Chem. Solids*, **57**, 443 (1996).
33. Alexeev A.N., Karpov S.Yu., Maiorov M.A., Myachin V.E., Pogorelsky Yu.V., Sokolov I.A. *J. Cryst. Growth*, **166**, 167 (1996).
34. L'vov B.V. *J. Therm. Anal. Calorium*., **96**, 487 (2009).
35. Bäuerle D. *Laser Processing and Chemistry* (Berlin–Heidelberg–New York: Springer, 2000).
36. Dubreuil B., Gibert T. *J. Appl. Phys.*, **76**, 7545 (1994).
37. Claeyssens F., Cheesman A., Henley S.J., Ashfold M.N.R. *J. Appl. Phys*., **92**, 6886 (2002).
38. Brewer P.D., Zinck J.J., Olson G.L. *Appl. Phys. Lett.*, **57**, 2526 (1990).
39. Abe K., Eryu O., Nakashima S., Terai M., Kubo M., Niraula M., Yasuda K. *J. Electron. Mater*., **34**, 1428 (2005).
40. Garcia K.K., Lindner H., von Bohlen A., Vadla C., Niemax K. *J. Anal. Atom. Spectrom.*, **23**, 470 (2008).
41. Aubriet F., Poleunis C., Muller J.-F., Bertrand P. *J. Mass Spectrometry*, **41**, 527 (2006).
42. Kukreja L.M., Rohlfing A., Misra P., Hellinkamp F., Dreiswerd K. *Appl. Phys. A*, **78**, 641 (2004).
43. McLoughlin C., Hough P., Costello J., Mosnier J.-P. *Appl. Surf. Sci*., **255**, 5338 (2009).
44. Bulgakov A.V., Predtechensky M.R., Mayorov A.P. *Appl. Surf. Sci*., **96-98**, 159 (1996).
45. Bulgakov A.V., Bobrenok O.F., Kosyakov V.I. *Chem. Phys. Lett*., **320**, 19 (2000).
46. Marine W., Bulgakova N.M., Patrone L., Ozerov I. *Appl. Phys. A*, **79**, 771 (2004).
47. Anisimov S.I., Imas Ya.A., Romanov G.S., Khodyko Yu.V. *Deistvie izlucheniya bol'shoi moshchnosti na metally* (Effect of High-Power Radiation on Metals) (Moscow: Nauka, 1970).
48. Batanov V.A., Bunkin F.V., Prokhorov A.M., Fedorov V.B. *Zh. Eksp. Teor. Fiz*., **63**, 586 (1972).
49. Tokarev V.N., Lunney J.G., Marine W., Sentis M. *J. Appl. Phys*., **78**, 1241 (1995).
50. Bulgakov A.V., Bulgakova N.M. *Kvantovaya Elektron.*, **27**, 154 (1999) [*Quantum Electron*., **29**, 433 (1999)].
51. Bulgakova N.M., Bulgakov A.V. *Appl. Phys. A*, **73**, 199 (2001).
52. Zhvavyi S.P., Zykov G.L. *Appl. Surf. Sci.*, **253**, 586 (2006).
53. Bulgakova O.A., Bulgakova N.M., Zhukov V.P., *Appl. Phys. A*, **101**, 53 (2010).
54. Samokhin A.A. *Tr. FIAN*, **13**, 3 (1988).
55. Miotello A., Kelly R. *Appl. Phys. Lett.*, **67**, 3535 (1995).
56. Anisimov S.I. *Zh. Eksp. Teor. Fiz*., **54**, 339 (1968).
57. Tmar M., Gabriel A., Chatillon C., Ansara I. *J. Cryst. Growth*, **68**, 557 (1984).
58. http://www.ioffe.rssi.ru/SVA/NSM/Semicond/InP/.
59. Kudman I., Steigmeier E.F. *Phys. Rev.*, **133**, 1665 (1964).
60. Itagaki K., Yamaguchi K. *Thermochim. Acta*, **163**, 1 (1990).
61. Zel'dovich Ya.B., Raizer Yu.P. *Physics of Shock Waves and High-Temperature Hydrodynamic Phenomena* (New York: Academic, 1966; Moscow: Nauka, 1966).
62. Itoh N. *Nucl. Instrum. Meth. Phys. Res. B*, **27**, 155 (1987).
63. Lazneva E.F. *Lazernaya desorbtsiya* (Laser Desorption) (Leningrad: Izd-vo Leningr. Univ., 1990).
64. Kanasaki J., Okano A., Ishikawa K., Nakai Y., Itoh N. *Nucl. Instrum. Meth. Phys. Res. B*, **101**, 93 (1995).
65. Wu Z. *Phys. Lett. A*, **131**, 486 (1988).
66. Sumi H. *Surf. Sci.*, **248**, 382 (1991).
67. Marine W., Bulgakova N.M., Patrone L., Ozerov I. *J. Appl. Phys.*, **103**, 094902 (2008).
68. Strekalov V.N. *Fiz. Tekh. Poluprovodn.*, **20**, 1939 (1986) [*Sov. Phys. Semicond*., **20**, 1218 (1986)].
69. Raff M., Schütze M., Trappe C., Hannot R., Kurz H. *Phys. Rev. B*, **50**, 11031 (1994).
70. Panish M., Arthur J. *J. Chem. Thermodyn.*, **2**, 299 (1970).
71. Lietoila A., Gibbons J. *J. Appl. Phys.*, **53**, 3207 (1982).
72. Vasil'ev V.P., Gachon J.-C. *Neorg. Mater.*, **42**, 1293 (2006).
73. Bulgakova N.M., Bulgakov A.V., Babich L.P. *Appl. Phys. A*, **79**, 1323 (2004).
74. Hagena O.F., Obert W. *J. Chem. Phys.*, **56**, 1793 (1972).
75. Golomb D., Good R.E., Balley A.B., Busby M.R., Dawbarn R. *J. Chem. Phys.*, **57**, 3844 (1972).
76. Beuhler R.J., Friedman L. *Nucl. Instrum. Meth.*, **170**, 309 (1980).

77. Hedén M., Kjellberg M., Bulgakov A.V., Hansen K., Campbell E.E.B. *Eur. Phys. J. D*, **43**, 255 (2007).
78. Reber A.C., Khanna S.N., Hunjan J.S., Beltran M.R. *Eur. Phys. J. D*, **43**, 221 (2007).
79. Al-Sunaidi A.A., Sokol A.A., Catlow C.R.A., Woodley S.M. *J. Phys. Chem. C*, **112**, 18860 (2008).
80. Campbell E.E.B., Hansen K., Hedén M., Kjellberg M., Bulgakov A.V. *Photochem. Photobiol. Sci.*, **5**, 1183 (2006).
81. Ye M., Grigoropoulos C.P. *J. Appl. Phys.*, **89**, 5183 (2001).
82. Moison J.M., Bensoussan M. *J. Vac. Sci. Technol.*, **21**, 315 (1982).
83. Raizer Yu.P. *Zh. Eksp. Teor. Fiz*., **37**, 1741 (1959).
84. Bulgakov A.V., Ozerov I., Marine W. *Thin Solid Films*, **453-454**, 557 (2004).
85. Gusev A.I. *Teplofiz. Vys. Temp.*, **29**, 695 (1991).
86. Godlevsky V.V., Derby J.J., Chelikowsky J.R. *Phys. Rev. Lett.*, **81**, 4959 (1998).
87. Wriedt H.A. *Bull. Alloy Phase Diagrams*, **8**, 166 (1987).
88. Shafer M., Weiser K. *J. Phys. Chem*., **61**, 1424 (1957).